Stratified Flow over Two-Dimensional Topography in Fluid of Infinite Depth: A Laboratory Simulation

PETER G. BAINES

CSIRO Division of Atmospheric Research, Aspendale, 3195, Australia

KLAUS P. HOINKA

DFVLR D-8031 Oberpfaffenhofen, West Germany

(Manuscript received 10 October 1984, in final form 12 March 1985)

ABSTRACT

This paper describes some laboratory experiments with two-dimensional stratified flow over isolated topography, in which a novel configuration simulating a radiating upper boundary condition is employed. Several experimental tests show that the upper boundary is quite effective in absorbing energy. The properties of flow over five different obstacle shapes were obtained for a range of values of the parameter Nh/U (h is obstacle height, N Brunt-Väisälä frequency and U towing velocity) from 0 to 4 (approximately). The main results of the study are 1) for $0 < Nh/U < 0.5$ (± 0.2), the flow is consistent with linear theory and Long's model; 2) for $0.5 \leqslant Nh/U \leqslant 2.0$, upstream columnar disturbances are found which apparently propagate arbitrarily far upstream in an inviscid system; 3) overturning and rotors in the lee wave field occur for $Nh/U \geqslant 1.5$; and 4) for $Nh/U \geqslant 2.0$, blocked fluid is present upstream, and in some cases is also apparent downstream. This upstream blocking is due to the superposition of the propagating columnar disturbances; it will similarly extend arbitrarily far upstream given sufficient time.

1. Introduction

The study of two-dimensional stratified flow over topography has a long history. The problem is best formulated by posing the question: What is the effect of introducing topography into flow which is otherwise known? We recognize two major types of stratified flow: 1) "finite depth," where the fluid is bounded above by an upper rigid boundary or an infinitely deep homogeneous layer, so that wave energy cannot escape vertically, and 2) "infinite depth," where internal waves which propagate upward are not reflected back. This latter type is probably the more relevant to the atmosphere, and it is the subject of this paper. It may be modeled by a fluid of finite depth below a region in which a radiation condition (implying no downward energy propagation) applies.

In inviscid finite depth situations it is by now firmly established that the introduction of topography often results in disturbances which may propagate indefinitely far upstream and permanently alter the flow which approaches the obstacle (Long 1955, 1970; Baines 1977, 1979a, b, 1984; Baines and Davies, 1980). For infinite depth flows, the situation in this respect is not so clear. Two analytical studies based on perturbation expansions in small obstacle height (McIntyre 1972), and in weak stratification about potential flow over finite obstacles (Baines and Grimshaw 1979), both show no permanent effects far upstream ("upstream influence") for obstacles introduced on a level surface. These solutions contain no singularities at special parameter values (which is a characteristic of linear solutions for finite-depth flows), and the higher order terms are similar in character to the first term in the respective expansions.

These solutions are also consistent with the solutions of "Long's model" [steady state solutions obtained when ρU^2 is constant with height far upstream where ρ is fluid density and U velocity, Long (1955)]. Miles (1968) and Huppert and Miles (1969) have obtained approximate solutions for flow over a number of different obstacle shapes using Long's model for infinitely deep fluids. Plausible flow fields were obtained for values of Nh/U (h is obstacle height and N the Brunt-Väisälä frequency far upstream) less than a critical value $(Nh/U)_c$, where the flow became statically unstable in the lee wave field. This critical value depended on the obstacle shape but was always of order unity. This model has been generalized in the simpler case of hydrostatic flow by Lilly and Klemp (1979), and for nonhydrostatic flow by Durran and Klemp (1983).

In many reports of numerical studies of stratified flow over isolated obstacles [Klemp and Lilly (1978), Clark and Peltier (1977), Peltier and Clark (1979)], no upstream influence has been described, values of Nh/U have typically been restricted to $Nh/U \leqslant 1.3$ and the studies have been focused on lee-side effects and downslope wind storms. All of these studies have rein-

forced the widespread assumption that disturbances which propagate upstream in infinitely deep stratified flows leak upward out of the system, and do not produce permanent effects far upstream at any level. More recently, upstream effects with continuous stratification have been investigated in the numerical studies of Pierrehumbert (1984) and Pierrehumbert and Wyman (1985); these models employ a sponge layer near the upper boundary, and the results suggest that upstream influence is possible in an infinitely deep domain.

Simple energy considerations (e.g., Sheppard, 1956) dictate that if Nh/U is sufficiently large, low-level flow upstream will be blocked and will not pass over the obstacle. It is also known that horizontally propagating disturbances are *possible* in infinitely deep stratified fluids. The equation for linear disturbances in a stratified flow is

$$\left(\frac{\partial}{\partial t} + U\frac{\partial}{\partial x}\right)^2 (w_{xx} + w_{zz}) + N^2 w_{xx} = 0, \qquad (1)$$

where x and z are horizontal and vertical coordinates, w is the vertical velocity, and the suffices denote derivatives. For disturbances of the form

$$w \sim \exp[i(kx + nz - \omega t)], \qquad (2)$$

the dispersion relation is

$$(\omega - Uk)^2 = \frac{N^2 k^2}{k^2 + n^2}. \qquad (3)$$

For waves of zero frequency the wavenumber surface (Lighthill 1967) is shown in Fig. 1, where the arrows

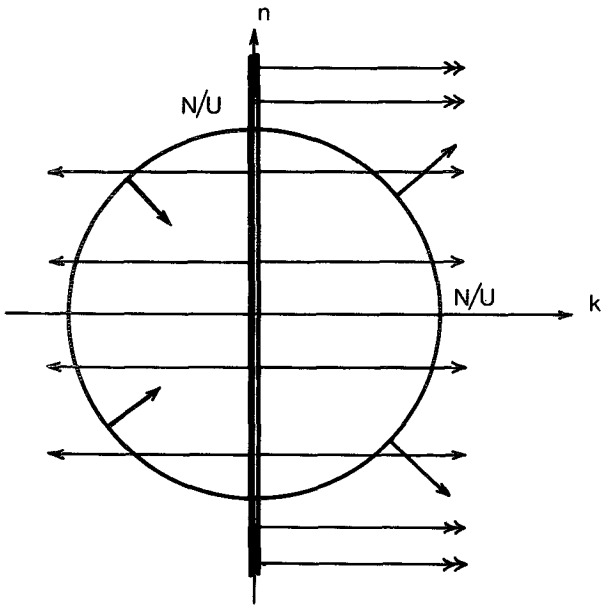

FIG. 1. The wavenumber surface for steady stratified flow of speed U incident from the left. The source is at the origin. The arrows are normal to the surface in wavenumber (k, n) space, and denote the directions of the corresponding group velocity in physical (x, z) space.

(normal to the surface in wavenumber space k, n) point in the direction in *physical* space of the group velocity of waves with that wavenumber. Hence, waves with wavenumbers $(0, n)$ where $0 < |n| < N/U$ may propagate upstream. The question is, how, and under what circumstances, does flow over an isolated obstacle *generate* them, and how are they related to upstream blocking?

This paper describes some laboratory experiments in which a new technique for simulating the upper radiation condition of "infinite depth" is employed. Other techniques have been tried by others with limited success and, to our knowledge, none of these attempts has been reported in the literature. The present technique is quite successful according to several criteria; it is described in detail in Section 2. In these experiments, isolated obstacles were towed down a long tank filled with stationary stratified fluid, starting from rest near one end. Five different obstacle shapes were used and a wide range of Nh/U values covered for each obstacle. We believe that our experiments establish, unequivocally, that permanent upstream effects (upstream influence) due to horizontally propagating waves may be produced by isolated obstacles in infinite depth systems when motion is commenced from a state of rest. For the obstacles employed here, permanent upstream motions appeared to be present for $Nh/U > 0.5$.

The experiments also indicate that upstream blocking (i.e., upstream "stagnant" fluid, stationary relative to the obstacle) is caused by these waves, and that it is present for $Nh/U \gtrsim 2.0$, although some degree of dependence of this value on obstacle shape was detected. The details of the observations, including other features such as wave-induced critical layers, are described in Section 3. Some comparisons with Long's model solutions are shown in Section 4 and the results are summarized in Section 5.

A note on terminology. In this paper the principal dimensionless number is Nh/U. There is no commonly accepted name for this number. Miles (1969) has suggested calling it the Russell number, and it or its reciprocal have been termed a Froude number by some authors (Baines included). In fact, there is little justification for the latter, and it seems appropriate to reserve the term "Froude number" for quantities which may be expressed as (fluid speed/wave speed), which is an extension of conventional engineering terminology. The number U/Nh or its reciprocal do not satisfy this criterion, and we leave them nameless in this paper.

2. Experimental arrangement—The upper boundary condition

The experiments were performed in a tank 9.17 meters long, 0.38 meters high, and 0.23 meters wide, which had been used for a number of other topographic studies (e.g., Baines 1979a, 1979b, 1984). For the present experiments the tank was modified by inserting a ver-

tical wall lengthwise along the tank leaving a gap of 8.75 cm from one side wall. This internal wall was 25 cm high and approximately 10 cm shorter than the tank, leaving a gap of 5 cm at each end (Fig. 2a). The tank was filled to a depth of approximately 34 cm, and a barrier, angled at 45° to the horizontal and extending the whole length of the tank, was inserted above the narrower of the two regions separated by the internal wall (Fig. 2b). The base of this angled barrier intersected the side wall at a height equal to that of the internal wall. Obstacles were towed along the bottom of this narrower region, and the flow was observed from the side.

The obstacles used in the experiments were placed on a tray 72 cm in length, which was towed along the bottom of the narrow section of the tank. These obstacles were uniform across this section except for a gap approximately 2 mm at each side. The obstacle height h given below is the total height of the obstacle above the tank floor (i.e., obstacle plus tray), but this does not include any allowance for the displacement thickness of the boundary layer on the obstacle as has been done for some previous experiments in Baines (1979b). This is because the obstacles were not long on the upstream side (with one exception), and also for consistency. In some cases, for example, an extensive region of blocked flow developed upstream, which created problems in defining a suitable consistent boundary layer thickness.

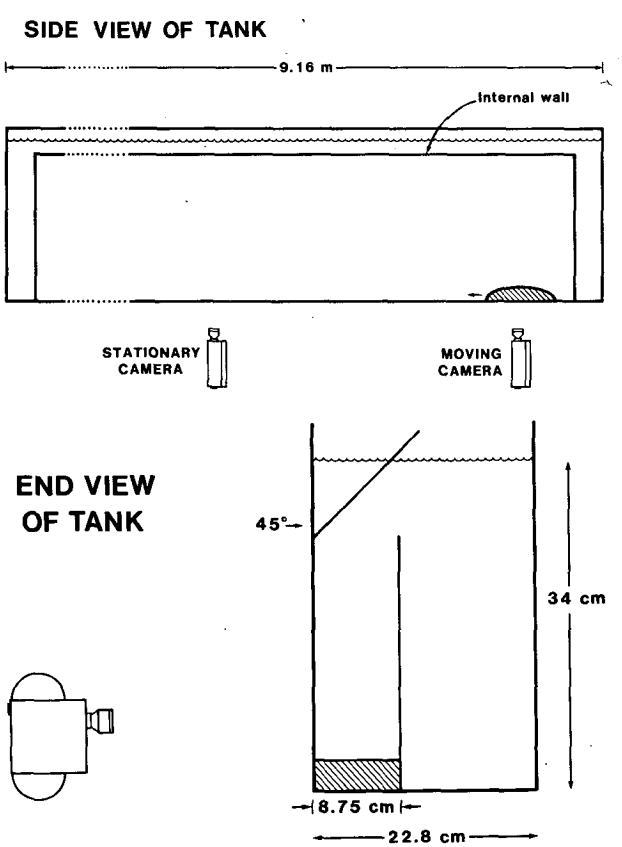

FIG. 2. Schematic diagram of the experimental arrangement.

The tank was filled with stratified fluid with constant density gradient using the customary two-tank method. Density variations were less than 4%, so that the Brunt-Väisälä frequency was effectively constant, and it had values that were close to unity. Flow visualization was achieved by using neutrally buoyant polystyrene beads which had a range of densities covering that of the stratified fluid. The density profile was checked regularly, as several runs were made with each fill, and the data recorded photographically, as in previous experiments. Time exposures yielded streak photographs and hence velocity fields.

The geometrical arrangement described in Fig. 2, models the upper radiation condition in the following manner. Motion of the obstacle will generate two-dimensional disturbances (no y-dependence), whose energy will propagate vertically. The waves will then encounter the three-dimensional geometry shown at the top of Fig. 2b. The equation governing three-dimensional linear internal waves in fluid at rest is,

$$\frac{\partial^2}{\partial t^2}(w_{xx} + w_{yy} + w_{zz}) + N^2(w_{xx} + w_{yy}) = 0, \quad (4)$$

for the vertical velocity w, where N is the Brunt-Väisälä frequency defined by

$$N^2 = -\frac{g}{\bar{\rho}}\frac{d\bar{\rho}}{dz}, \quad (5)$$

where $\bar{\rho}(z)$ is mean density. For an upward-propagating component with frequency ω and wavenumber component k in the x-direction, ω and k will remain constant in the subsequent motion (if we ignore the ends of the tank). For a component of the form

$$w = \hat{w}(y, z)\exp[i(kx - \omega t)], \quad (6)$$

we therefore obtain

$$\hat{w}_{yy} - c^2\hat{w}_{zz} - k^2\hat{w} = 0, \quad (7)$$

where

$$c^2 = \omega^2/(N^2 - \omega^2).$$

This is a Klein–Gordon equation, which governs the across-tank structure of the disturbances. When the vertically propagating waves reach the upper part of the two-dimensional channel there will be some degree of wave energy reflected back into the channel, due to a mismatch of impedances between the channel and the region above it. This effect is difficult to calculate, and the observational evidence indicates that it is insignificant in these experiments. We therefore assume, for the present discussion, that virtually all the vertically propagating wave energy in the channel escapes into the upper region. Vertically propagating waves in the x–z plane will be affected by two main factors in the upper part of the tank—diffraction above the central

barrier into the wider region of the tank, and reflection from the upper angled barrier. We now discuss these phenomena in turn.

Diffraction past a vertical barrier which is aligned parallel to the direction of wave propagation in the manner already described has not been described previously in the literature. A simplified version of the problem is analyzed here in the Appendix, in order to describe the character of the wave motion in the upper portion of the tank. For the main results, we refer to Fig. 3a. A vertically propagating incident wave component will have the form

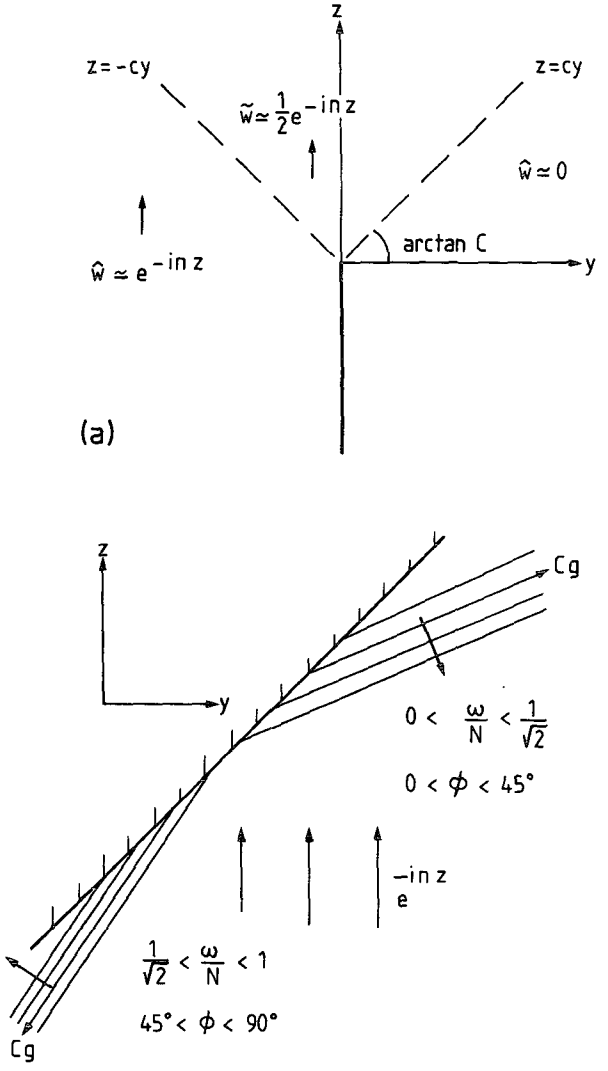

FIG. 3. (a) Diffraction of vertically propagating internal waves past the central barrier: behavior in the y–z plane. (b) Reflection of vertically propagating waves from the angled upper surface: behavior in the y–z plane.

$$\hat{w} = e^{-inz}, \tag{8}$$

where $n > 0$ if $\omega > 0$, and k may have either sign; for definiteness we assume $\omega > 0$ and $k > 0$. For $z < -cy$, the incident wave is largely unaffected by the barrier. For $z > c|y|$ the wave has half the amplitude of the incident wave, plus an evanescent term with y-dependence which decays with height as $(1/kz)^{1/2}$. There is no effective penetration of the wave into the region $y > z/c$. Inviscid singularities occur on the junctions of these regions $z = \pm cy$, but these have no consequences for our present discussion. A substantial fraction of the wave energy is therefore "diffracted" across the barrier, and the wave above the narrow region of the tank may be reduced by up to 50% in amplitude but without significant change in its structure.

Above the narrow region the vertically propagating wave component (8) will encounter the angled barrier and be reflected as another plane wave of the form

$$\mathbf{u} = \mathbf{u}_R \exp[i(kx + l_R y + n_R z - \omega t)], \tag{9}$$

where μ is the fluid velocity and μ_R a constant vector, satisfying

$$\mathbf{k}_R \cdot \mu_R = 0,$$

where

$$\mathbf{k}_R = (k, l_R, n_R). \tag{10}$$

The boundary condition of zero normal velocity and the dispersion relation give (for barrier angle 45°),

$$l_R = 2\frac{(\omega/N)^2}{1 - 2(\omega/N)^2}, \quad n_R = -\frac{n}{1 - 2(\omega/N)^2}, \tag{11}$$

and the reflected waves are illustrated in Fig. 3b. For $l_R > 0$ ($0 < \omega/N < 1/\sqrt{2}$) the reflected wave propagates over the central barrier into the wider region of the tank. For $l_R < 0$ ($1/\sqrt{2} < \omega/N < 1$) the wave is reflected back into the narrow operating region. However, we expect this backward reflection to have a negligible effect on our observations for the following reasons: 1) the group velocity of the reflected wave vanishes at both ends of this range, so that for frequencies near these values downward propagation will be negligible and the wave will be dissipated near the reflecting barrier; 2) for the steady-state wave pattern given by equations (1)–(3) and illustrated in Fig. 1, waves with $1/\sqrt{2} < Uk/N < 1$ are found downstream of the obstacle. The downward-reflected wave components all have smaller group velocities (in both x and z directions) than the incident waves, and hence they will be present even farther downstream of the wave pattern generated by an isolated obstacle; 3) any downward-reflected waves will have a significant y-component, and this will preclude their forming modes with the upward-propagating components.

For the waves which pass over the central barrier, once they enter the broader region of the tank they will generally have very long travel times (being reflected down to the bottom and back again) so that

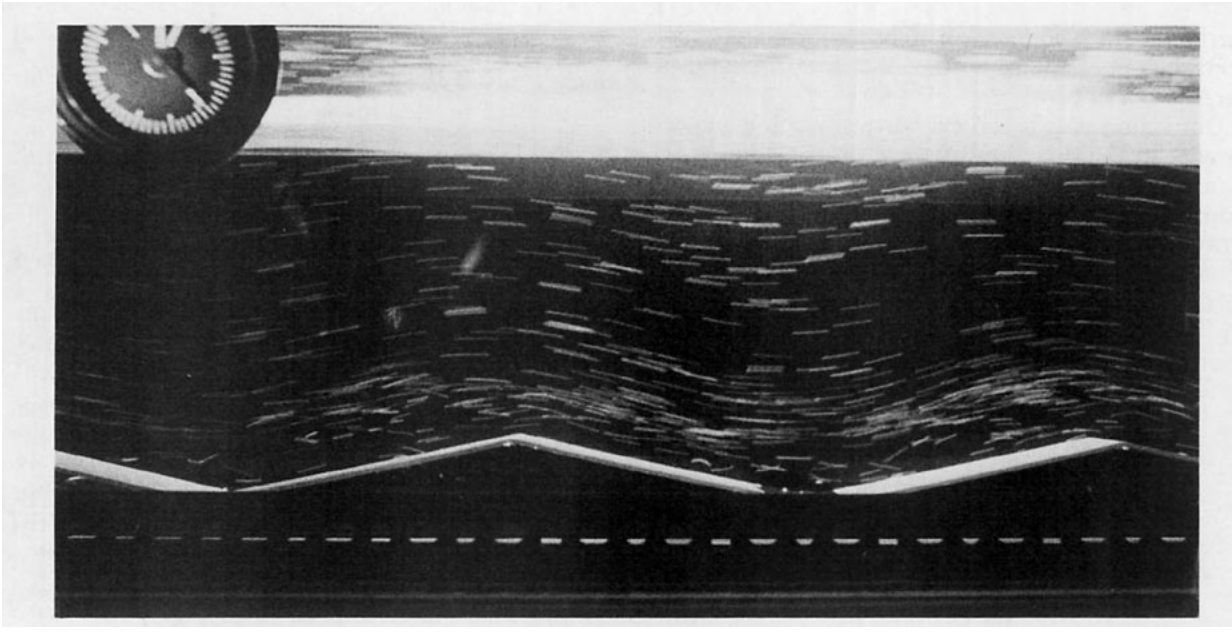

FIG. 4. An example of flow over the periodic saw-tooth topography; $Nh/U = 0.89$. Note the forward tilt of the phase lines with height.

they are either dissipated there or return long after the observations in the narrower region have been made.

This simulated radiation condition was tested experimentally by towing two types of periodic topography through the tank and comparing the resultant wave motion with that expected on theoretical grounds for a perfectly absorbing upper boundary. The upward-propagating wave has the same horizontal period as the topography, and we compare the observed slope of the phase lines with the theoretical slope $\tan\theta = k/n = k/[(N/U)^2 - k^2]^{1/2}$. The periodic topographies used were sinusoidal (6 periods, wavelength 14.8 cm) and sawtooth (6 periods, wavelength 40.4 cm). An example with the latter topography is shown in Fig. 4; here, as in the other cases examined, there is no evidence of downward reflection or three-dimensional structure, even though this topography is extensive in the horizontal rather than localized. Results for various different towing speeds (frequencies) are shown in Fig. 5; the agreement with theoretical phase angles indicates that the upper radiation condition is modeled quite well, although there is a tendency for the observed angles θ to be larger than the theoretical values for large θ.

The $\sim$5 cm gap in the central barrier at each end of the tank had the effect of reducing the reflection of the low-frequency upstream motions apparently to zero. Several tests were made for reflected motions but none could be detected. The upstream waves propagated "around the corner" into the broader region, so that the tank acted as a race track type for these motions. This effect was not, however, relied upon heavily in these experiments, as most observations were completed before the obstacle came within 2.5 m of the upstream end of the tank, but it certainly prolonged the effective development time for the flow, relative to a "rigid-ended" tank.

3. Observations with a single obstacle

Approximately 130 observational runs were made with five different obstacle shapes, covering Nh/U values ranging from approximately 0 to 4. Details of the obstacles are given in Table 1. Most of these runs were photographed using both the stationary and moving still cameras, and were also recorded on video tape with a stationary camera. This substantial body of recorded data has been stored at Aspendale; it is described here in summary form.

We first describe the motion observed upstream of the obstacles. An overall view is shown in Fig. 6. For $Nh/U < 0.5$ (± 0.2), no upstream motion was observed, other than very close to the obstacle where displacements were forced by continuity. For $Nh/U > 0.5$ (± 0.2), however, columnar wave motions with conspicuous horizontal but very small vertical velocity were observed propagating upstream. These had similar character to those described in Baines (1977, 1979a) for the same flow situations but in finite-depth fluids, except that in the present experiments no vertical modes were discernible in the flow. Instead the spectrum of horizontal motion in the vertical was broadband and continuous. This was quite apparent in the evolution of the upstream velocity profile. At a fixed distance upstream of the obstacle, the disturbances first arrived with extremely large vertical wavelength (somewhat greater than the actual depth of the fluid); as time increased, progressively smaller-scale waves arrived, and the velocity profile became more oscillatory

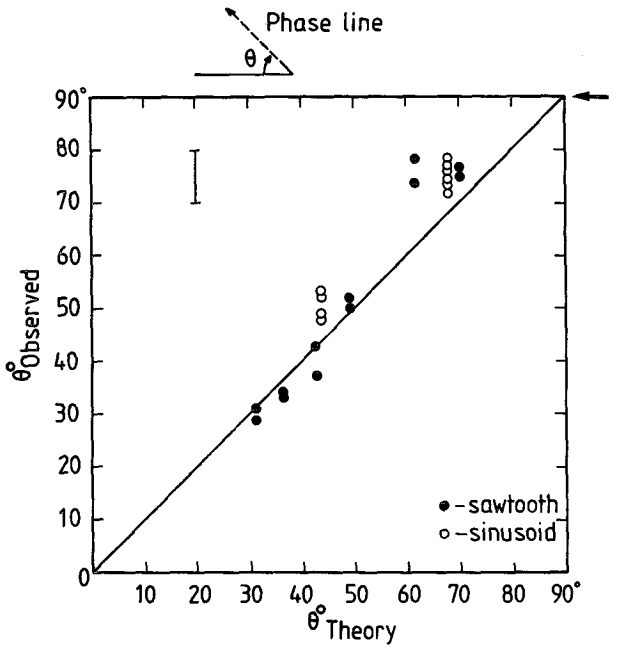

FIG. 5. Observed vs theoretical phase angles for periodic topography. The arrow (top right) indicates the expected phase for a rigid reflecting upper boundary.

with the "oscillations" moving downward. The time evolution of this velocity profile was continuous, and no sudden variations in its rate of change, suggesting the presence of discrete (or even leaky) modes, could be detected. The large error bars at $Nh/U = 0.5$ reflect the difficulty in separating the propagating columnar disturbance from the evanescent upstream part of the linear solution, which has very similar vertical structure, in these towing experiments with their limited operating time.

Most of the runs were commenced with a sudden start to the motion of the obstacle. To test for the possible effect of this on the generation of transients, some runs were made in which the obstacle commenced motion slowly, reaching constant speed after a distance of approximately 1.5 m. When observations were made farther upstream, no differences in the upstream development or in the final profile were evident. The decrease in the approach velocity (relative to the obstacle) at lowest levels, for example, was always monotonic. This suggests that upstream transient features (which *were* evident in finite-depth situations) propagate upward out of the system, whereas the (ultimately) steady columnar motions do not. Velocity profiles measured at a point immediately upstream of the obstacle are shown in Fig. 7, for four obstacles (1 to 4 in Table 1) for a range of Nh/U values. These profiles were measured after the obstacle had covered a distance of 4 m or more. In each case a number of pictures were taken, and the profiles shown are each the mean of three or four realizations, with the error bars indicating the mean magnitude of the scatter. For small Nh/U the scatter was smaller than the error bars, but it increased as Nh/U increased; it was larger than the error bars for the largest Nh/U values shown. Inspection of the photographs indicated that at this location the flow had reached an *approximately* steady state (although this was not the case for points farther upstream at the same time). The absence of any discernible trend with time in the measured profiles supported this view, but the fact that the velocity observations were more scattered for $Nh/U > 2$ makes the attainment of steady state less certain in this range. However, a consistent picture emerges from these averaged profiles showing, as Nh/U increases, velocity profiles with decreasing wavelength and descending fluctuations. The development of the blocked region, together with the jet above the level h and its decreasing scale with increasing Nh/U, can be clearly seen. Little variation with obstacle shape was apparent for $Nh/U < 2$. [Note the difference in scale between a and b ($h \sim 3$ cm) and c and d ($h \sim 6.5$ cm).]

The maximum velocity in the steady state profiles measured immediately upstream of the semielliptical obstacle is shown in Fig. 8 as a function of Nh/U. This quantity has been chosen as a measure of the magnitude of the upstream disturbances. For this purpose, it is superior to the velocity minimum near the ground in these experiments, because measurement of the latter is complicated by technical factors—a paucity of beads, and the viscous effects of the towing cable and the lower boundary. These results suggest that the onset of the upstream motion as Nh/U increases above 0.3 occurs

TABLE 1.

Obstacle	Number	Height h* (cm)	Shape	a (cm)	Comments
Semicircle	1	3.3	$h[1 - (x^2/a^2)]^{1/2}$	3.0	
Semi-ellipse	2	2.9	$h[1 - (x^2/a^2)]^{1/2}$	8.3	
Witch of Agnesi	3	6.5	$h/[1 + (x^2/a^2)]$	4.0	
W of A/Ramp	4	6.8	$h/[1 + (x^2/a^2)]$ Near-plane ramp, slope 0.12	4.0	Left-hand side Right-hand side
Ramp/W of A	5	6.8			Obstacle 4 reversed

* Note that h here denotes the total height, including the supporting tray.

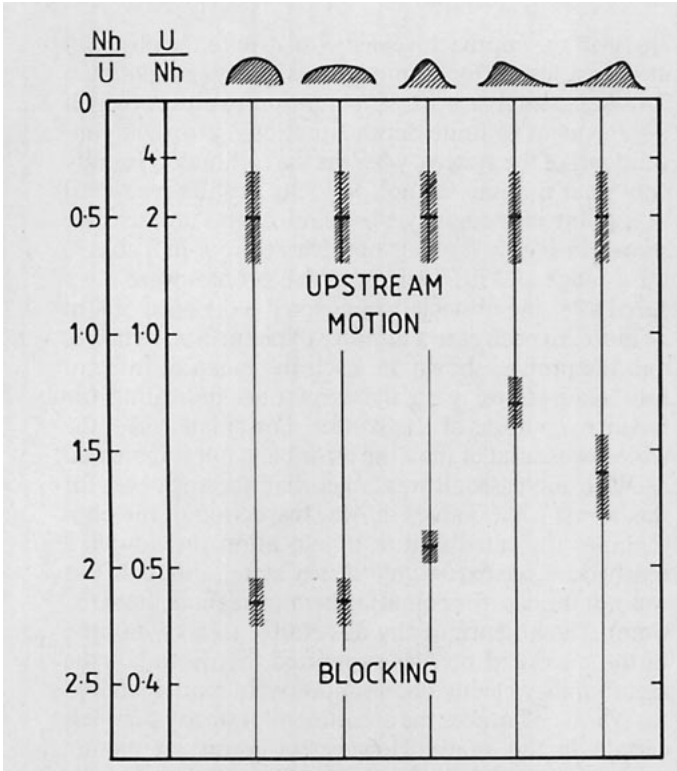

FIG. 6. Criteria for the presence of columnar upstream motion and upstream blocking in terms of Nh/U for the given obstacle shapes used, and denoted above each line. The hatched regions denote error bars.

continuously from zero, within the limits of observational error.

As Nh/U increased beyond 0.5, the magnitude of the upstream disturbances at the lowest levels increased until the fluid became blocked; i.e., it was stationary relative to the obstacle. The value of Nh/U at which this occurred is shown in Fig. 6; it varied somewhat with obstacle shape, but was typically about two. Measurement of the depth of the blocked region was somewhat inaccurate due to the technique used (observing streak photographs), but when blocking first appears (i.e., $Nh/U \sim 2$) the depth is approximately 1/2 h. This depth increased slightly as Nh/U increased further. On the basis of these observations, therefore, the onset of blocking occurs when a slowly moving layer of finite thickness is brought to rest, rather than by first forming a blocked layer of near zero thickness, which then grows upward. This process is consistent with the wave propagation mechanism, when the upper limit to the contributing vertical wavenumbers is N/U. These blocked regions may be seen clearly in Fig. 9, particularly for the taller obstacles in c, d, and e.

Figure 9 displays the nature of the flow over each of the five obstacles for a range of values of Nh/U. Lee waves of fairly large-scale are evident for $Nh/U < 1.5$. For $Nh/U \geq 1.5$, a region of very small velocity—a "stagnant patch" or "rotor"—is evident, embedded in the lee wave field immediately downstream of the obstacle. This critical value for Nh/U for overturning (~ 1.5) is not precise, but it does not seem to be very sensitive to obstacle shape. For obstacles 1–4 (Table 1) the height H_s of the stagnant region when it first forms is

$$H_s \sim 3h \sim (Nh/U)\lambda/2 \sim 3\lambda/4, \qquad (12)$$

where $\lambda = 2\pi U/N$. This is approximately the height of overturning as given by linear theory (e.g., Peltier and Clark, 1979), although the observed flow is now significantly nonlinear. Peltier and Clark also obtained the same height for overturning in their nonlinear computations, although their value of Nh/U was slightly smaller (1.3). For the fifth obstacle the initial overturning region is somewhat lower ($<2h$). As Nh/U increases, this stagnant region tends to spread horizontally above the lee side of the obstacle. This constitutes the "wave-induced critical region" found in the numerical computations by Peltier and Clark. As is evident from Fig. 9, as Nh/U increases further the critical region generally becomes slightly lower; the lee wave amplitude above this level becomes quite small, but it is still substantial below the critical level (or region). These low-level lee waves are sited on a region of velocity maximum or "jet," which comes from just above the blocked (or nearly blocked) region upstream. Since the blocked flow region has weak density gradients, this low-level jet region must have an enhanced density gradient which supports these waves.

Another property evident from Fig. 9 is that blocked flow upstream is generally accompanied by blocked flow downstream; the downstream blocked layer has comparable but generally smaller thickness, and both layers are surmounted by the low-level jet. We did not concentrate on downstream flow features in this study, but one very striking phenomenon observed several times is shown in Fig. 10. In this example, for the W of A shaped obstacle with $Nh/U = 0.79$, two or more humps filled with stagnant fluid (in the frame of the obstacle) were present downstream, with a very pronounced and thin (but stable) shear layer at their upper surface. The same phenomenon was observed for $Nh/U = 0.9$ and 1.1.

In some cases significant lee-side separation was observed, e.g., in Fig. 9c. No obvious correlation between such separation and upstream disturbances was apparent in these experiments.

4. Comparison with Long's model solution

Differences between the observed flows and the solutions obtained from Long's model are apparent from Section 3. To illustrate this further, we here present two comparisons of flow fields for semicircular (Fig. 11a) and semi-elliptical obstacles with minor/major axis = 0.3 (Fig. 11b), for values of Nh/U for which the Long's model streamlines become vertical somewhere (approximately). The Long's model solutions are taken from Miles (1968) and Huppert and Miles (1969), re-

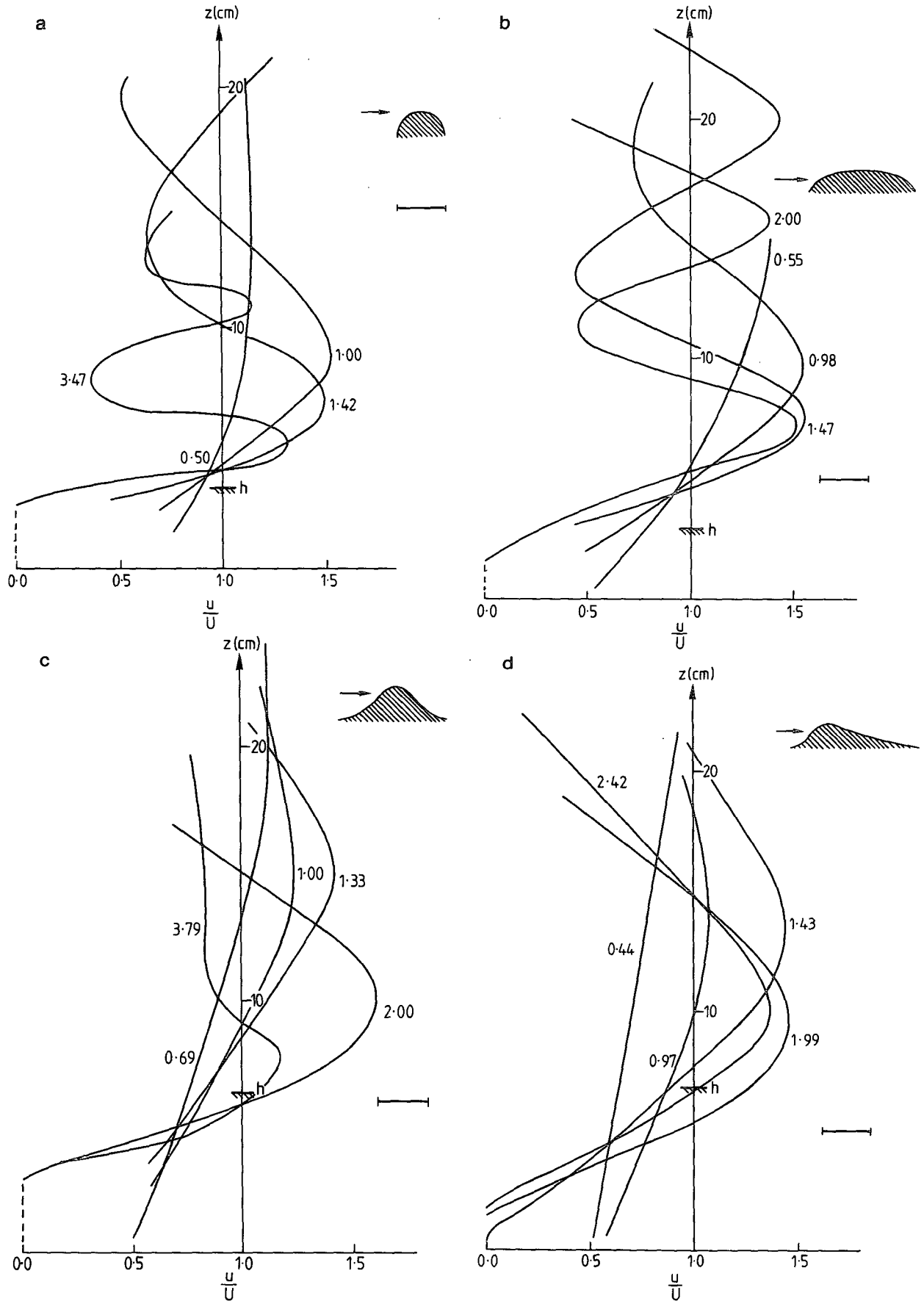

FIG. 7. Horizontal velocity profiles measured immediately upstream of the obstacles towards the end of the runs where the flow had reached an approximately steady state. The numbers denote values for Nh/U. Each curve is the mean of three or four realizations for the same run. (a) Semicircle, (b) Semi-ellipse, (c) Witch of Agnesi, (d) Witch of Agnesi/ramp.

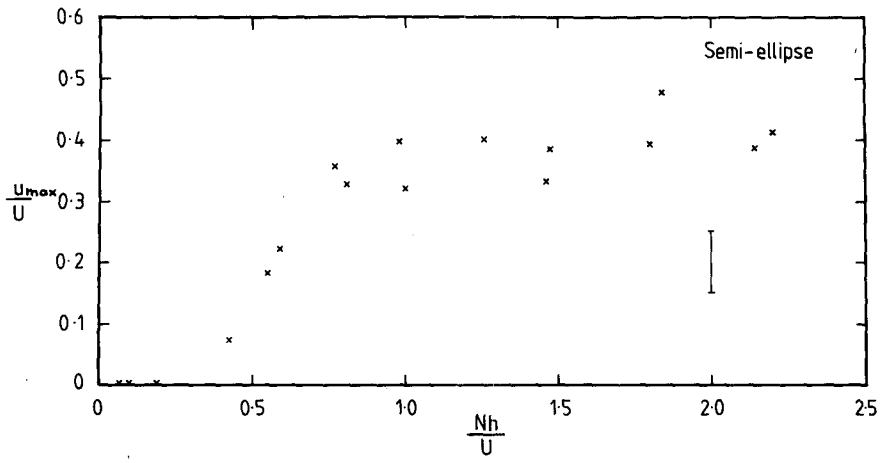

FIG. 8. Maximum horizontal fluid velocity (in the laboratory frame) measured immediately upstream of the semi-elliptical obstacle (2 in Table 1) after (apparently) locally steady state has been reached, as a function of Nh/U.

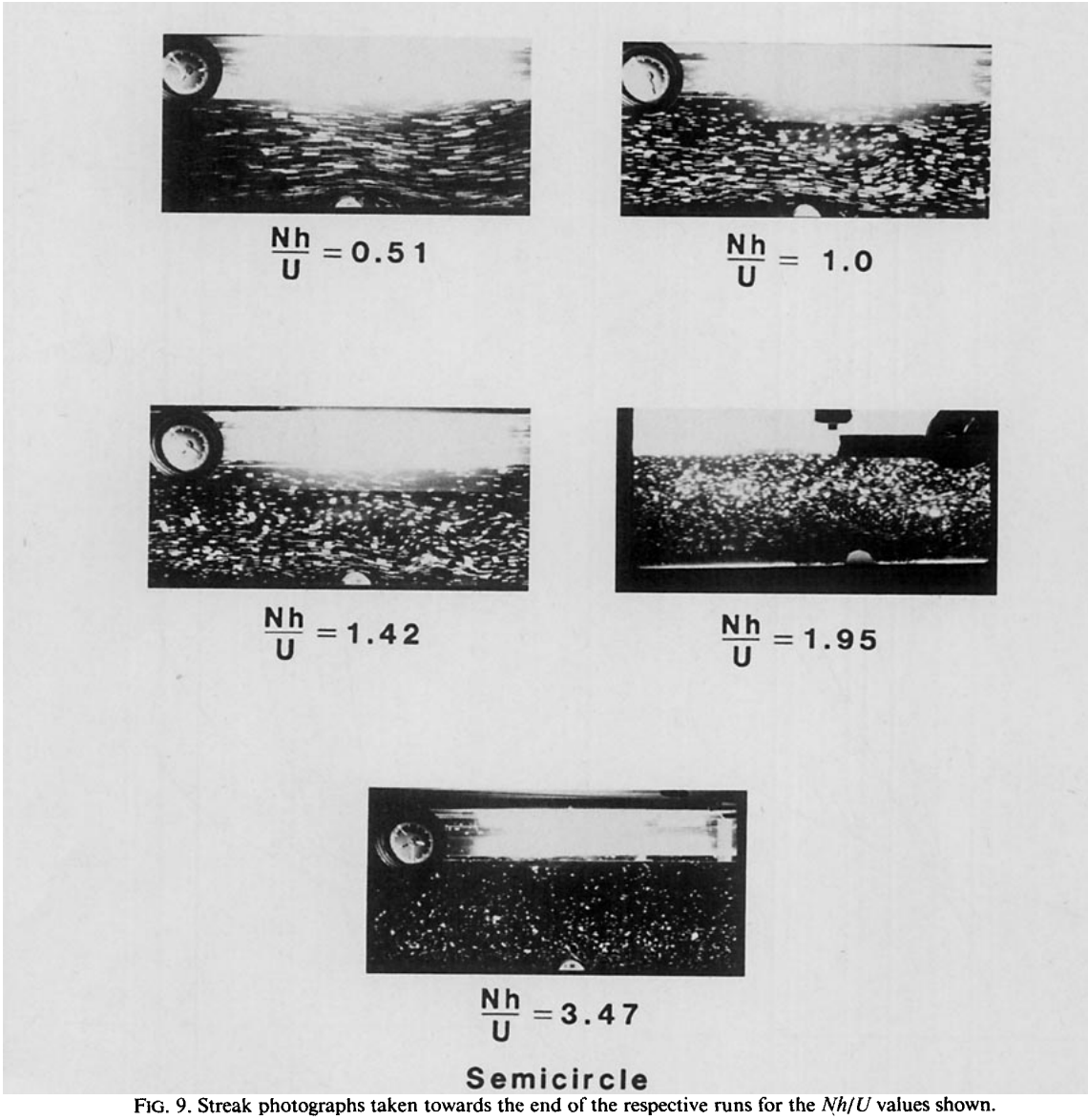

FIG. 9. Streak photographs taken towards the end of the respective runs for the Nh/U values shown.

spectively, and are approximations based on two terms in an infinite series of lee wave functions. These two terms give an adequate representation of the series for the total wave drag and the wave scattering cross section, so that the approximation to the detailed wave field is probably adequate.

Note that the nonuniform upstream velocity profiles are evident in the observations, but absent from the theory. However, the most obvious difference between these two sets of pictures is that the observed lee-wave amplitude is substantially smaller than that given by Long's model. Vertical streamlines do not appear in the experiments until Nh/U is somewhat larger (~ 1.5) than the values shown here.

5. Discussion and conclusions

We have described some laboratory experiments that simulate the flow of stratified fluid over isolated obstacles, with a radiating upper boundary condition. On the basis of theoretical considerations and a number of experimental tests, we believe this simulation to be quite successful; no evidence of downward reflection of energy could be detected.

Five different obstacle shapes were towed through initially stationary stratified fluid, starting from rest. The resulting observed flow properties may be conveniently described in terms of ranges of values of the parameter Nh/U.

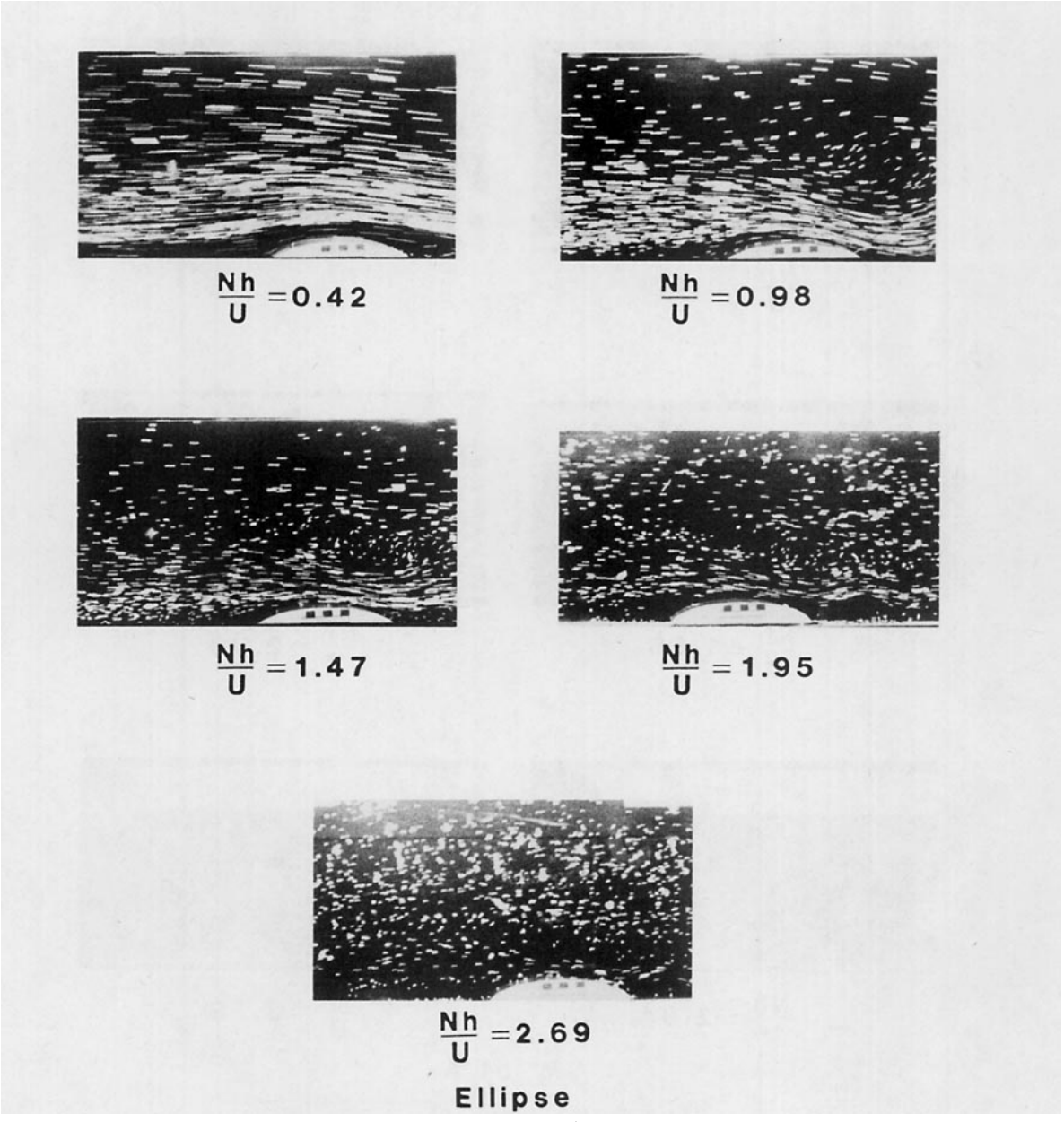

FIG. 9. (*Continued*)

1) $0 < Nh/U < 0.5\ (\pm 0.2)$. In this range, the observed "steady state" flow consists of lee waves downstream with wavenumbers of order N/U, and no significant disturbances upstream. The flow appears to be quite consistent with linearized flow solutions and Long's model solutions, except that separation may occur if the lee side of the topography is sufficiently steep. Within the limits of its determination, the upper limit of this range ($Nh/U = 0.5$) was not sensitive to obstacle shape.

2) $0.5\ (\pm 0.2) < Nh/U \lesssim 2.0$. In this range, horizontally propagating long wave ("columnar") disturbances are observed propagating ahead of the obstacle. The observed upstream propagation speed is consistent with the expression

$$C = N/n - U, \quad k = 0, \tag{13}$$

(positive in the upstream direction) for the speed relative to the obstacle, so that upstream propagation is possible for wavenumbers $n < N/U$. The largest-scale waves travel fastest and $C \to 0$ as $n \to N/U$. At a fixed point upstream of the obstacle, therefore, one observes a continuous change in the horizontal velocity profile as progressively smaller-scale waves arrive. Each part of this continuous spectrum reduces the horizontal ve-

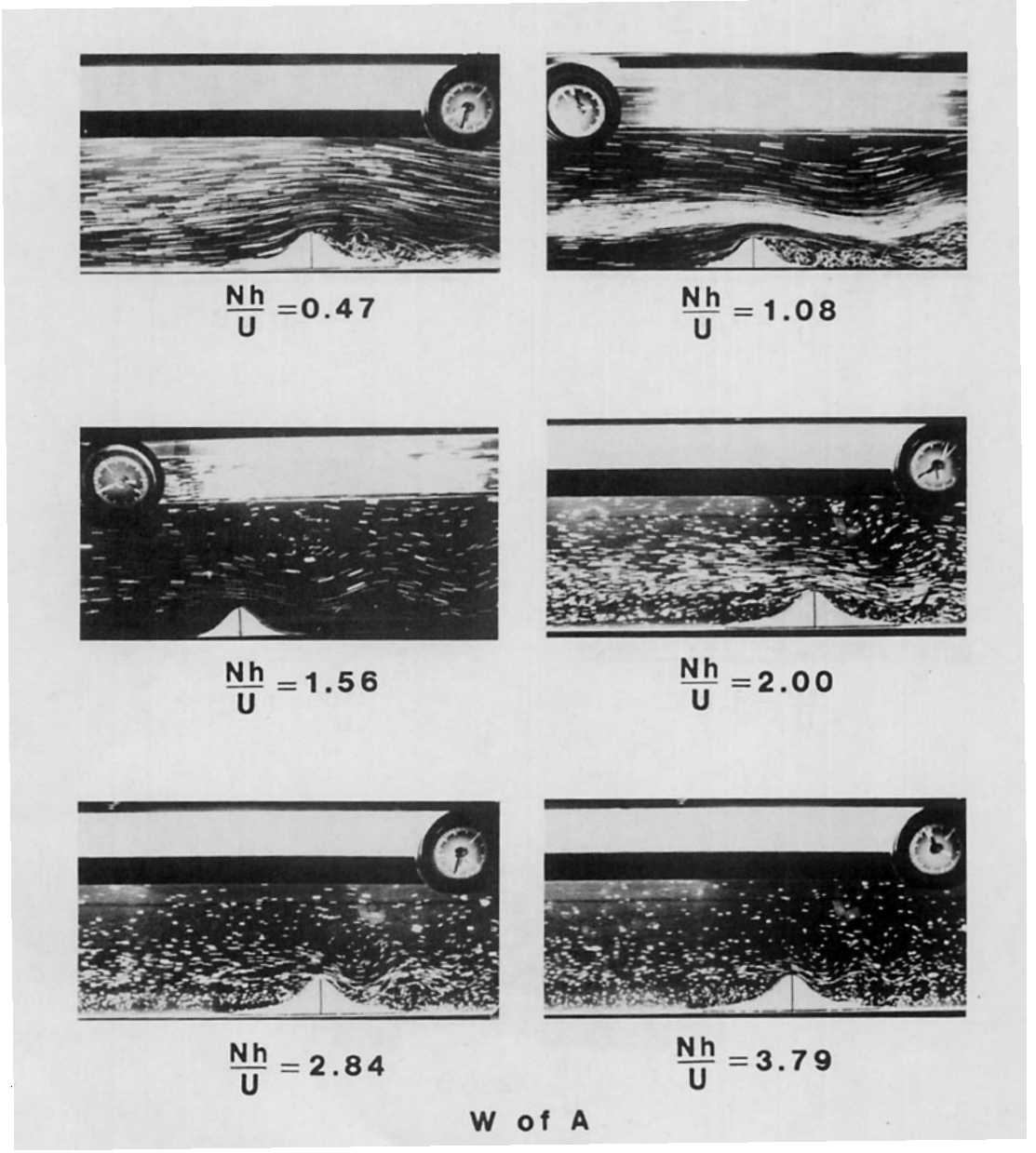

FIG. 9. (*Continued*)

locity of the approaching fluid near the ground, and increases it in a jet above the blocked region. We infer from the observations that, if dissipative effects are excluded, these upstream disturbances would propagate arbitrarily far upstream and establish a steady velocity profile there, although it may take a very long time for the components with $n \sim N/U$ to arrive. As Nh/U increases from 0.5 to 2, the approach velocity near the ground decreases from U to near zero. Over the obstacle the lee waves progressively steepen as Nh/U increases and overturning commences at $Nh/U \sim 1.5$, and this value is relatively insensitive to obstacle shape. This results in semistagnant regions ("rotors") embedded in the lee wave field where the fluid separates and passes both above and below, as described in Baines (1977) for finite depth flow. As Nh/U increases further, the lowest (and most significant) stagnant region tends to spread horizontally above the lee-side of the obstacle. This effectively creates a wave-induced critical layer at this level z_c (which is typically at height $3h$). Above the level z_c the wave amplitude is now significantly smaller than it is for smaller Nh/U, whereas for $z < z_c$ the wave amplitude may still be large in the jet region.

3) $Nh/U \gtrsim 2.0$. In this range, some low-level fluid on the upstream side is blocked (i.e., stagnant), and the value at which this occurs may vary slightly with

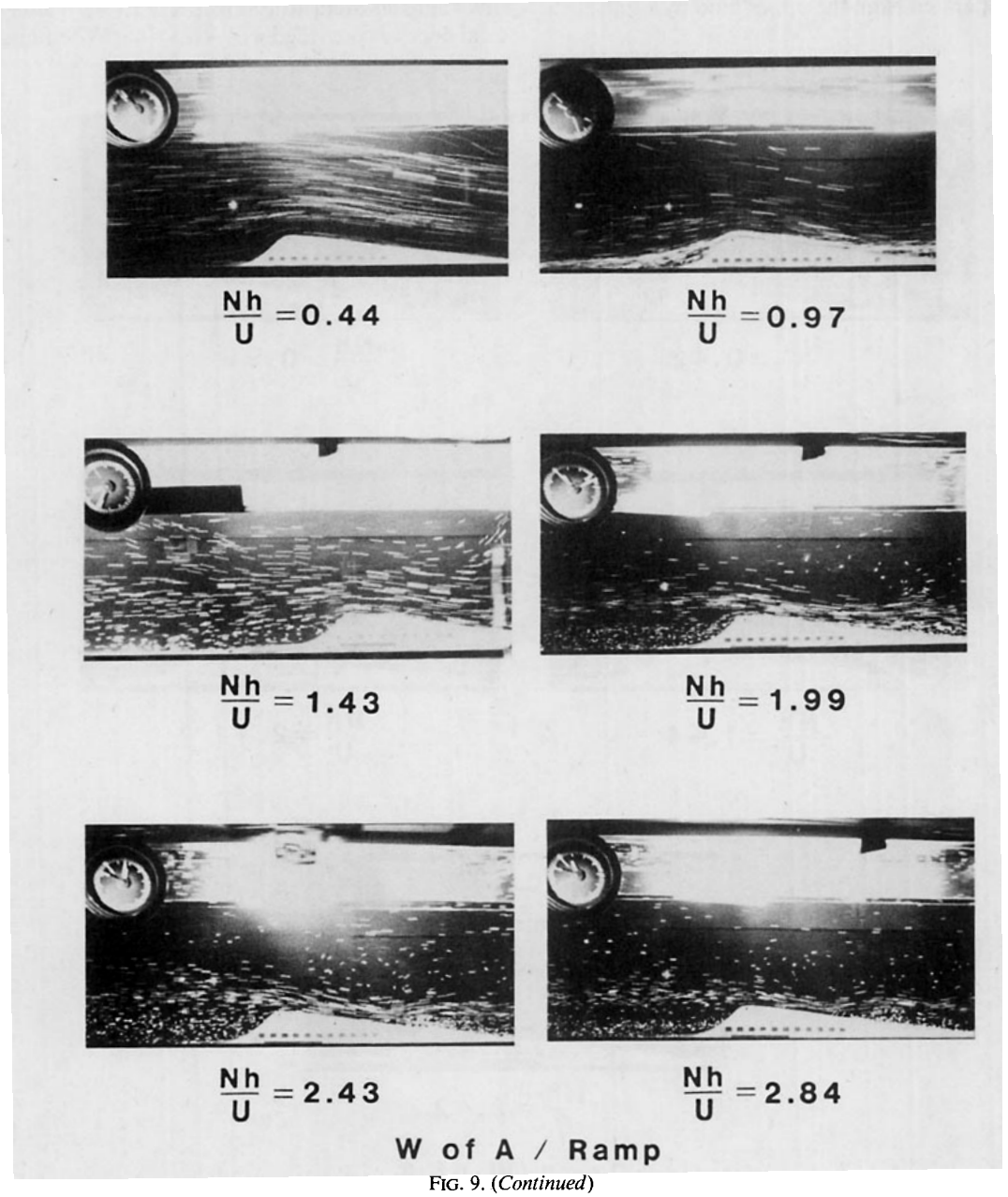

FIG. 9. (*Continued*)

obstacle shape. As time increases, the region of blocked fluid extends farther upstream and tends to a constant depth (which depends on obstacle shape and Nh/U). This upstream blocking is produced by the superposition of the upstream columnar disturbance modes. We suggest that this mechanism can explain and describe such blocking in all stratified systems where viscosity is a minor factor. The critical layer observed when $Nh/U < 2$ at $z \sim z_c$ persists; lee-wave amplitudes may be large for $z < z_c$, but are very small for $z > z_c$. Downstream, at low levels, blocking (i.e., fluid moving with the obstacle) is also evident. In some cases this has a wavy structure and consists of a sequence of "bulges" separated from the upper fluid by a thin shear layer.

These experiments were restricted to $Nh/U \leqslant 4$, but at the upper end of this range the flow had some properties which approximated those expected at the limit $Nh/U \rightarrow \infty$, namely, blocked flow upstream and downstream for $z < h$, and a viscous shear layer at $z = h$, and relatively quiescent flow above. This suggests that the parameter range of these experiments covers most of the interesting phenomena in the transition from Nh/U small to Nh/U large.

The foregoing results for *blocking* may be compared with those described for finite depth cases in Baines 1979b for a Witch of Agnesi-shaped obstacle. The criterion for blocking obtained was also $Nh/U \geqslant 2.0$, and this value showed little sensitivity to the value of the total depth D provided $\pi U/ND < 0.5$. When upstream

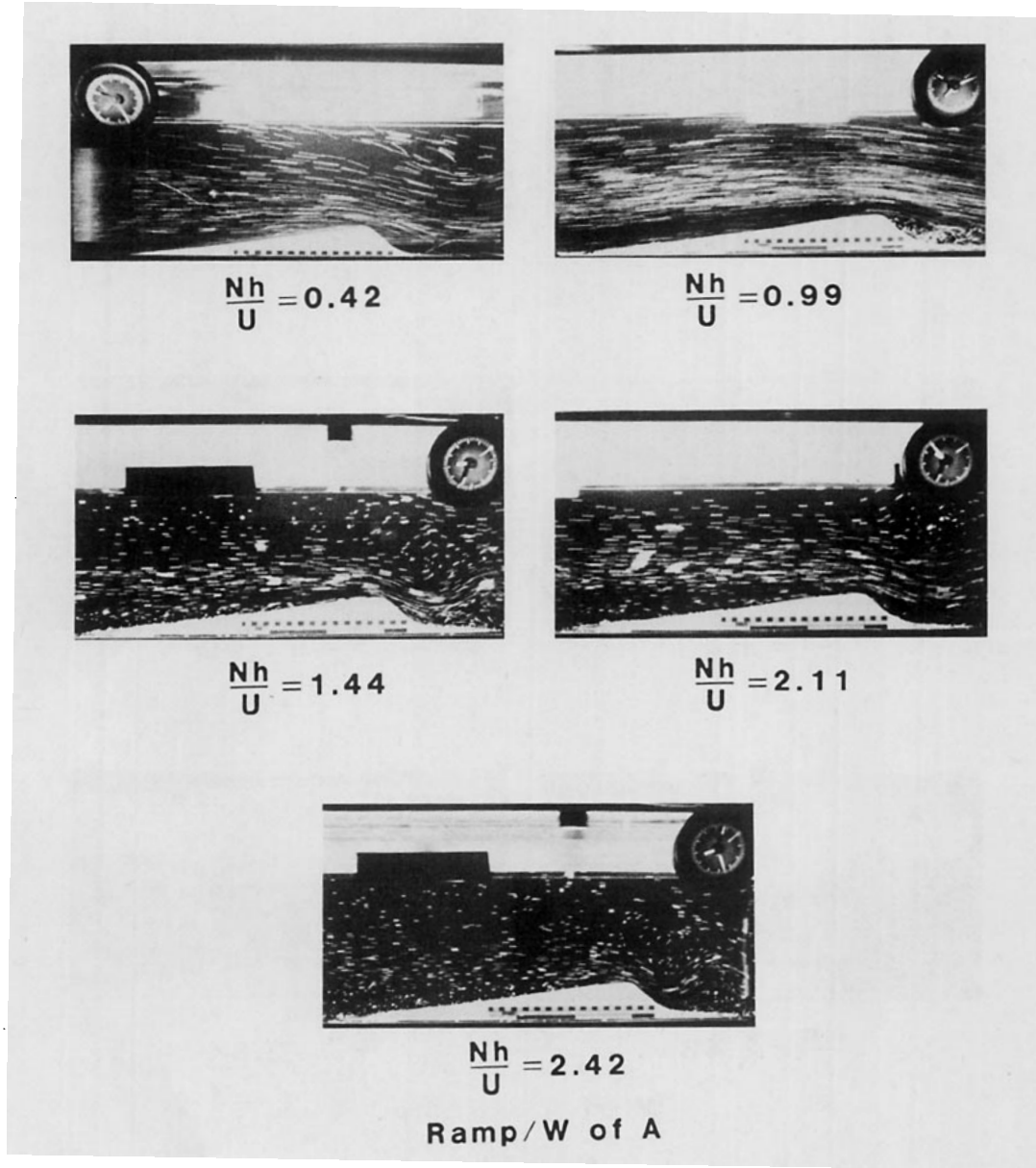

FIG. 9. (*Continued*)

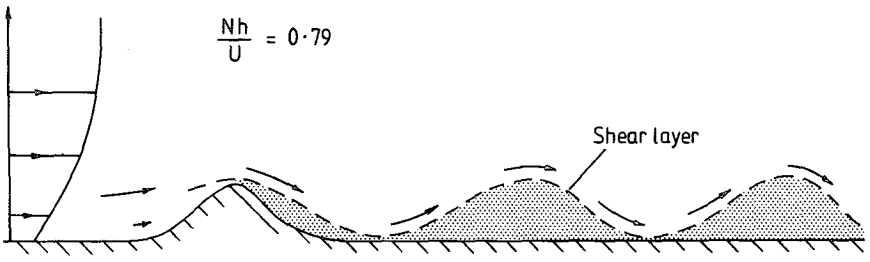

FIG. 10. Diagram showing the stationary humps observed in the lee of the Witch of Agnesi.

blocking first occurred, the depth of the blocked layer was comparable with $h/2$; this is also found in the present experiments, as is evident in the pictures of Fig. 9 where $Nh/U \sim 2$. With regard to upstream blocking, therefore, the results for finite depth (with a discrete vertical wave spectrum) have much in common with those for infinite depth (with a continuous spectrum). This suggests that when $\pi U/ND$ is small, we may expect finite depth systems to behave similarly to infinite depth ones, with regard to these phenomena. It follows that we may expect the results of Baines (1979b) for flow past three-dimensional barriers to be applicable in the infinite-depth case also. In particular, for a two-dimensional mountain barrier with narrow gaps, if $Nh/U \geqslant 2$ the low-level nearly blocked fluid flows horizontally through the gaps and has a depth $[z \sim h(1 - 2U/Nh)]$ which depends on Nh/U; at the upper boundary of this region, there is an abrupt change (manifested as a shear layer) to a flow region in which the fluid flows over the topography in an approximately two-dimensional fashion.

It was remarked in Section 1 that earlier numerical studies have not reported upstream effects of the kind described here. However, an inspection of Figs. 6 and 7 of Peltier and Clark (1979), where $Nh/U = 1.3$, clearly shows phenomena of this type propagating upstream. We, therefore, believe that these effects are, in fact, present in the numerical models, but have gone unnoticed partly because they have not been expected. They are most readily seen in the horizontal velocity profiles, whereas numerical model outputs have tended to concentrate on streamlines and vertical velocities. The recent computations by Pierrehumbert (1984) and Pierrehumbert and Wyman (1985) do describe the upstream disturbances, and with nonrotating hydrostatic flow with two-dimensional topography, totally blocked flow is found upstream for $Nh/U > 2.0$ (± 0.5).

A dimensionless parameter which has not been varied systematically in the present experiments is the ratio h/L, where L is a measure of the obstacle length, although some variation is implicit in the different obstacle shapes used. The ratio may be combined with Nh/U to give NL/U; for each obstacle shape, the value of this parameter will govern lee-side separation and the degree of hydrostaticity of the flow. For example, for $Nh/U \leqslant 1$ these experiments are all nonhydrostatic, but they become progressively more hydrostatic as Nh/U increases. The hydrostatic results of Pierrehumbert and Wyman (1985) show differences from the present ones when $Nh/U \leqslant 1$ (most notably, the point of onset of upstream disturbances), but they are, substantially, in agreement for $Nh/U \geqslant 2$.

If we wish to relate the results of the present experiments to atmospheric situations, for example, flow over the European Alps, we must consider the effects of the two major approximations; namely 1) two-dimensional topography and 2) nonrotating flow. Firstly, the results of Baines (1979b) discussed above imply that low-level fluid which is blocked in the two-dimensional situation will flow horizontally around an extensive three-dimensional barrier, whereas fluid above this blocked region will flow over the barrier. We believe that this same phenomenon is observed in the Alpex data (e.g., Pierrehumbert 1984, Fig. 1), in the form of the shear layers upstream at heights close to 3 km. Secondly, scale analysis dictates that the effects of rotation locally on the flow will be small if the mean time taken for a fluid particle to pass across the topography is much less than an inertial period, i.e., $R_0 = U/fL \gg 1$, where L is the characteristic width of the mountain range and f the Coriolis frequency. This condition is satisfied in many atmospheric situations. In all cases, however, rotation will affect the upstream propagation distance of the upstream disturbances. The effects of rotation are discussed in some detail by Pierrehumbert and Wyman (1985).

At present no theoretical model which can explain and describe the mechanism of the generation of these upstream motions exists for infinite depth systems. The studies of McIntyre (1972) and Baines and Grimshaw (1979) show that this generation process must be nonlinear. Also, the similarity between the finite and infinite depth observations described above indicates that this generation process is probably also similar in these two situations. For hydrostatic flow in the finite depth case, conditions over the obstacle are governed by a "critical flow" condition (Baines 1984 and recent unpublished work) which controls the amplitude of the upstream disturbances. It, therefore, appears plausible that the vertically periodic flow (Lilly and Klemp, 1979) which is set up by the disturbances produced when Nh/U is small in the infinite-depth case, establishes an

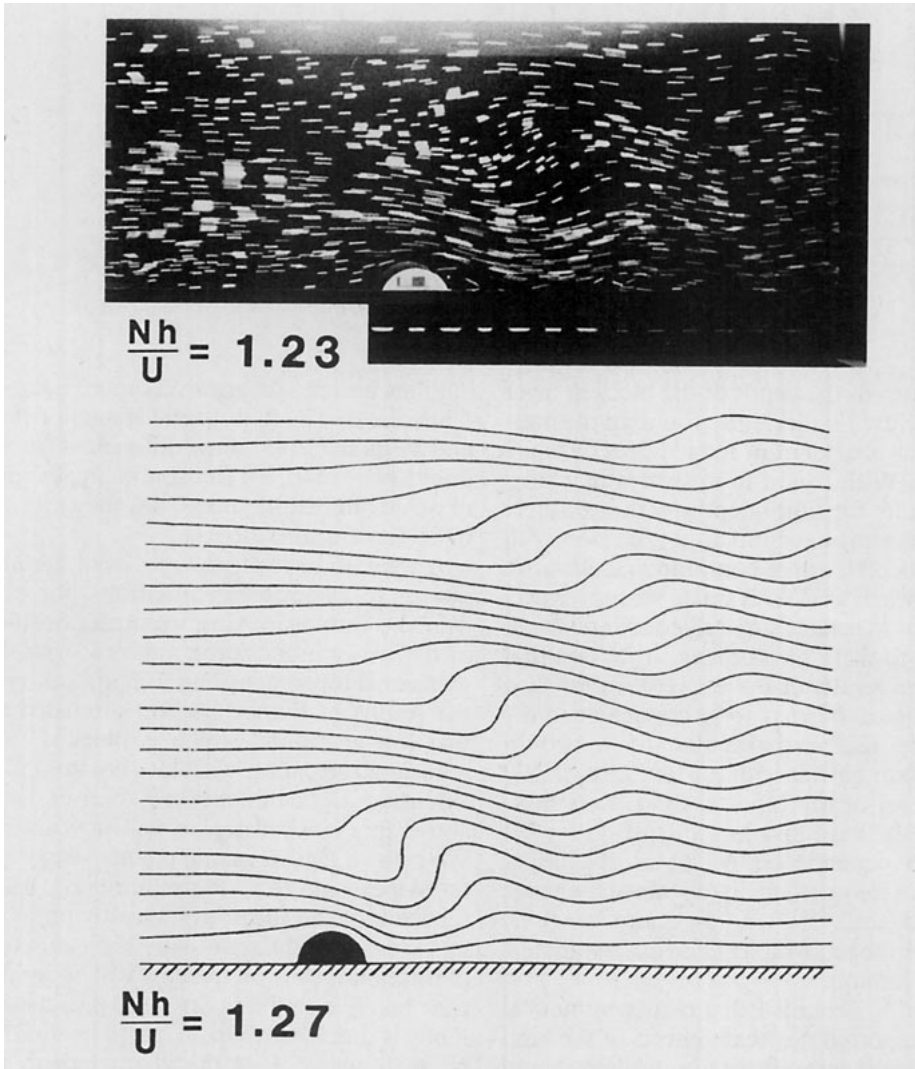

FIG. 11. Comparison between the observed flows (late in run, and therefore near steady state) and Long's model solution for the Nh/U value at which the latter is marginally statically unstable. (a) Semicircle, (b) Semi-ellipse with $h/a = 0.3$.

"effective" critical flow condition, at least for hydrostatic flow.

APPENDIX

Diffraction of an Internal Wave Past a Horizontal Knife-Edge Aligned Parallel to the Incident Wave

We address this problem by solving instead a simpler version that specifies the boundary conditions on the plane surface $z = 0$. The main objective is to describe the general character of the wave motion in the region $z > 0$. This model problem is

$$\hat{w}_{yy} - c^2\hat{w}_{zz} - k^2\hat{w} = 0, \tag{A1}$$

with

$$\hat{w} = \begin{cases} \exp(-inz + \epsilon y), & -\infty < y < 0, \quad z = 0 \\ 0, & y > 0, \quad z = 0 \end{cases}, \tag{A2}$$

and a radiation condition at large z; ϵ is introduced for mathematical convenience, is small and positive, and will be reduced to zero subsequently.

Introducing

$$\bar{w}(l, z) = \int_{-\infty}^{\infty} e^{-ily}\hat{w}dy, \tag{A3}$$

we obtain

$$\bar{w}_{zz} + \frac{k^2 + l^2}{c^2}\bar{w} = 0 \tag{A4}$$

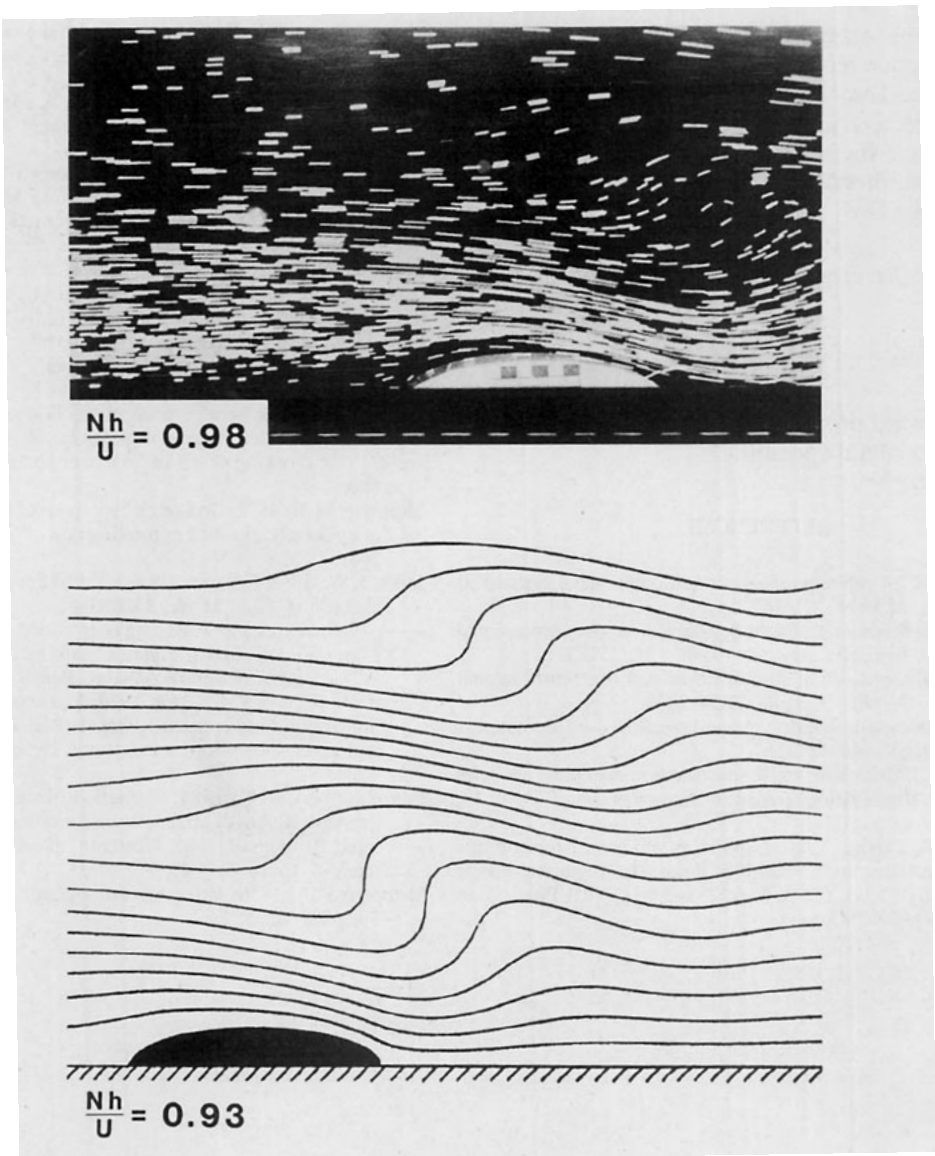

FIG. 11. (*Continued*)

so that

$$\bar{w} = A \exp[-i(k^2 + l^2)^{1/2} z/c] + B \exp[i(k^2 + l^2)^{1/2} z/c]. \quad \text{(A5)}$$

The radiation condition of no incoming internal wave energy requires that

$$B = 0, \quad \text{(A6)}$$

and the conditions at $z = 0$ then imply

$$A = \frac{1}{\epsilon - il}. \quad \text{(A7)}$$

Inverting the Fourier transform then gives

$$\hat{w}(x, z) = \frac{1}{2\pi} \int_{-\infty}^{\infty} \frac{e^{ily}}{\epsilon - il} \exp[-i(k^2 + l^2)^{1/2} z/c] dl. \quad \text{(A8)}$$

This integral may be evaluated using standard techniques to give

$$\begin{aligned} \hat{w} &= \frac{1}{\pi} \int_1^{\infty} \frac{e^{-kys}}{s} \cdot \sinh(s^2 - 1)^{1/2} kz/c \cdot ds, \quad y > z/c, \\ &= e^{-inz} + \frac{i}{\pi} \int_1^{\infty} \frac{e^{-kys}}{s} \sinh(s^2 - 1)^{1/2} kz/c \cdot ds, \\ &\qquad y < -z/c, \quad \text{(A9)} \\ &= \frac{1}{2} e^{-inz} - \frac{i}{\pi} \int_0^1 \sinh kys \cdot \exp[-i(1 - s^2)^{1/2} kz/c] \frac{ds}{s} \\ &\qquad + \frac{1}{\pi} \int_1^{\infty} \sinh kys \cdot \exp[-(s^2 - 1)^{1/2} kz/c] \frac{ds}{s}, \\ &\qquad |y| < z/c, \\ &= \frac{1}{2} e^{-inz} + I_1 + I_2. \end{aligned}$$

For $|y| > z/c$ the integrals contain no phase propagation terms, and hence represent no energy propagation in the y–z plane. They have singularities of the form $1/|y \pm z/c|$ respectively.

For $|y| < z/c$ the second integral I_2 is of the same type. The first integral I_1 may be approximated when $|ky| \ll 1$ by

$$I_1 = -\frac{ky}{2}\left(J_1(kz/c) - Y_1(kz/c) + \frac{2}{\pi}\int_0^\infty \sinh s \exp(-kz/c \sinh s)ds\right) + O(ky)^3, \quad \text{(A10)}$$

giving an upward propagating wave which decays with height due to lateral spreading.

REFERENCES

Baines, P. G., 1977: Upstream influence and Long's model in stratified flows. *J. Fluid Mech.*, **82,** 147–159.

——, 1979a: Observations of stratified flow over two-dimensional obstacles in fluid of finite depth. *Tellus,* **31,** 351–371.

——, 1979b: Observations of stratified flow past three-dimensional barriers. *J. Geophys. Res.*, **83,** 7834–7838.

——, 1984: A unified description of two-layer flow over topography. *J. Fluid Mech.*, **146,** 127–167.

——, and R. H. J. Grimshaw, 1979: Stratified flow over finite obstacles with weak stratification. *Geophys. Astrophys. Fluid. Dyn.*, **13,** 317–334.

——, and P. A. Davies, 1980: Laboratory studies of topographic effects in rotating and/or stratified fluids. In Orographic Effects in Planetary Flows, Chap. 8, p. 233–299. GARP Publication No. 23, WMO/ICSU.

Clark, T. L., and W. R. Peltier, 1977: On the evolution and stability of finite amplitude mountain waves. *J. Atmos. Sci.*, **34,** 1715–1730.

Durran, D. R., and J. B. Klemp, 1983: A compressible model for the simulation of moist mountain waves. *Mon. Wea. Rev.*, **111,** 2341–2361.

Huppert, H. E., and J. W. Miles, 1969: Lee waves in a stratified flow. Part 3, semi-elliptical obstacle. *J. Fluid Mech.*, **35,** 481–496.

Klemp, J. B., and D. K. Lilly, 1978: Numerical simulation of hydrostatic mountain waves. *J. Atmos. Sci.*, **35,** 78–107.

Lighthill, M. J., 1967: On waves generated in dispersive systems by travelling forcing effects, with application to the dynamics of rotating fluids. *J. Fluid Mech.*, **27,** 725–752.

Lilly, D. K., and J. B. Klemp, 1979: The effects of terrain shape on nonlinear hydrostatic mountain waves. *J. Fluid Mech.*, **95,** 241–261.

Long, R. R., 1955: Some aspects of the flow of stratified fluids. III. Continuous density gradients. *Tellus,* **7,** 341–357.

——, 1970: Blocking effects in flow over obstacles. *Tellus,* **22,** 471–480.

McIntyre, M. E., 1972: On Long's hypothesis of no upstream influence in uniformly stratified or rotating flow. *J. Fluid Mech.*, **52,** 209–243.

Miles, J. W., 1968: Lee waves in a stratified flow. Part 2. Semi-circular obstacle. *J. Fluid Mech.*, **33,** 803–814.

——, 1969: Waves and wave drag in stratified flows. *Proc., 12th Int. Congress of Applied Mechanics,* Stanford (Eds., M. Hetenyi and W. G. Vincenti). Springer-Verlag, Berlin.

Peltier, W. R., and T. L. Clark, 1979: The evolution and stability of finite-amplitude mountain waves. Part II. Surface wave drag and severe downslope windstorms. *J. Atmos. Sci.*, **36,** 1498–1529.

Pierrehumbert, R. T., 1984: Formation of shear layers upstream of the Alps. Rivista di Meteorologia Aeronautica, (to be published).

——, and B. Wyman, 1985: Upstream effects of mesoscale mountains. *J. Atmos. Sci.*, **42,** 977–1003.

Sheppard, P. A., 1956: Airflow over mountains. *Quart. J. Roy. Meteor. Soc.*, **82,** 528–529.